Applicability of hyperspectral fluorescence imaging to mineral sorting

Sebastian Bauer, Dominic Mann and Fernando Puente León

Karlsruhe Institute of Technology, Institute of Industrial Information Technology, Hertzstraße 16, 76187 Karlsruhe, Germany

Abstract Hyperspectral fluorescence images of mineral samples have been acquired. Their spatial and spectral structure is analyzed and the samples are classified. Mineral samples from the same deposit may show large spectral differences, while samples from different deposits can appear quite similar. These analyses are a good start into the research of using mineral fluorescence as sorting technique, but more effort has to be taken to come to satisfying classification results.

1 Introduction

There are quite a few techniques for mineral sorting, e.g., X-ray fluorescence and laser-induced breakdown spectroscopy (LIBS) [1, 2]. Most of them suffer from drawbacks like high cost or difficulties in handling, such as X-rays. In this article, the applicability of hyperspectral fluorescence imaging as alternative mineral discrimination technique is investigated. Fluorescence is the short-lived form of luminescence, which is the emission of light after optical excitation. Due to energy loss, the wavelength of the radiation emitted by the sample is longer than the excitation wavelength (so-called Stoke's shift) [3]. A small portion of chemical impurities (e.g., rare earth ions), the luminescent centers, also called activators, are responsible for the emission of fluorescence photons, and small amounts of other impurities such as Fe^{2+}, Co^{2+} and Ni^{2+}, the so-called quenchers, drastically reduce the intensity of the fluorescence [4]. Due to the fact that small amounts of impurities determine not only the intensity, but also the fluorescence color, specimens of the same mineral kind but of different locales can vary greatly in fluorescence intensity and color [5].

Hyperspectral fluorescence imaging has been used for determinining the state and constituents of food such as corn and apples [3,6,7], but to the best of our knowledge not yet been applied to mineral sorting. Kim et al. [8] describe a system for the hyperspectral analysis of fluorescence and reflectance combined with 3D analysis. Although they also examine minerals with their system, their main focus is on investigations of biological and fine arts issues such as the visual appearance and perception of birds. They do not consider the different fluorescence spectra of minerals for sorting applications. Fluorescence studies of minerals have been reported by Hofer et al. [9], however, they only measured point spectra. In this article, in contrast, we will describe hyperspectral fluorescence images. By acquiring hyperspectral images, it is possible to investigate space-resolved spectra of the samples and analyze the spatial variance of the investigated sample. The space-resolved acquisition of fluorescence spectra bears the potential of providing reliable means of mineral discrimination because more information, i.e., more spectra and the spatial relationship between them, can be analyzed. Therefore, e.g., smaller surface areas with and without skin can be analyzed.

2 Experimental setup

We already presented the first results of hyperspectral fluorescence imaging of a small set of mineral samples [10] as well as feasible image reconstruction techniques [11]. We now contribute an analysis of a larger sample number of more different mineral types and point out the spatial characteristics of the fluorescence radiation. Additionally, the spectra were recorded at a higher spectral resolution, i.e., 4 nm instead of 17 nm. We still use the same setup: Within a closed box, the samples are illuminated by a tunable monochromatic light source with a 300 W xenon arc lamp of which spectrum the interesting part is cut out by a 300 mm Czerny-Turner monochromator. The resulting light is directed to the sample by a high-reflectance aluminum mirror with about 85 % reflectance across the spectral range from 250 to 800 nm. The light emitted by the sample is filtered by an acousto-optical tunable filter (AOTF, Gooch&Housego HSi-300). This is a filter which transmits a certain wavelength at a selected bandwidth. Both wavelength and bandwidth can be adjusted almost arbitrarily between 450 and 800 nm,

while the smallest possible bandwidth is 1.5 nm. Such a filter allows for fast and flexible wavelength selection. The light that passed the filter is acquired by an Andor iXon$_3$ 897 EMCCD (electron multiplying charge-coupled device) with 512 $\times$ 512 pixels. In this type of camera, the photo electrons are multiplied electrically in an on-chip multiplication register before readout. For this reason, there is a higher signal level before the read noise is added. Although some noise is added during the multiplication process, the total SNR increases. Even the registration of single photons is possible when appropriate settings are used. Cooling the chip down to about −85 °C almost completely eliminates the dark current and allows for long exposure time spans, as the only relevant noise component is the time-independent read noise.

We chose excitation wavelengths from 260 to 360 nm in steps of 20 nm. The light source was running continuously. The spectral resolution of the acquired images is 4 nm with a bandwidth of 3.9 nm, resulting in a total of 86 pictures of the scene at wavelengths from 450 to 790 nm. In contrast to [10], the exposure time has been adjusted to take care of the varying spectral intensity of the light source such that regardless of the wavelength, the same number of photons is delivered to the samples. This results in exposure times per single image ranging from 24 to 112.8 s. A total of 33 minerals of 6 different mineral types originating from different natural mineral deposits was analyzed, see Table 17.1.

Table 17.1: Used minerals.

type	magnesite	talc	dolomite	granite	chlorite	quartz
number of samples	13	8	5	2	3	2

3 Fluorescence analysis

No pre-processing of the minerals such as cutting etc. was performed. All samples had a dust-free surface. The samples were split up into three scenes as the illumination spot was not big enough for all samples. A complete hyperspectral image of each scene was acquired. Each band's image was then filtered by the Hessian Schatten norm regularization method [12]. To correct for the spatially inhomogeneous illu-

mination, the spatial fluorescence intensity of white paper was measured. Each fluorescence image of the samples was divided by these corresponding spatial intensity values. The pixel spectra were corrected by taking the spectral sensitivity/transmission of the lens, the AOTF, the camera window and the EMCCD sensor into account. The numbers were taken from the supplied data sheets. There are, however, unknown correction factors that could not be figured out yet. They could be due to inaccurate parameter values automatically used by the software during the sweep.

Figure 17.1 shows the image of one scene acquired at 526 nm using 320 nm excitation wavelength. This image clearly shows the intensity differences of the fluorescence of the samples at the considered wavelength. After applying the image filtering, the sample contours can be seen better. Note that the two white magnesite samples (lower left corner) are the brightest, while there is quite a large intensity difference between them. Talc (last three samples in the top row and first four in the middle row) shows the second brightest fluorescence in this scene, even stronger than the yellow magnesite samples (last two samples in the middle row). Granite (two samples in the upper left corner) fluoresces at a very low intensity. It is mentionable that just like with the two white magnesites, there is an intensity difference between the two granite samples. The three chlorite samples in the lower right corner show almost no fluorescence.

As not all spectra can be presented here, the average spectra of each magnesite sample at 360 nm excitation wavelength are shown in Fig. 17.2. It can be seen that samples from different origins have different fluorescence spectra.

The acquired spectra cannot be compared to literature fluorescence spectra due to two reasons: Firstly, the previously mentioned unknown spectral correction factors, and secondly, the fluorescence spectra depend on the natural mineral deposits the samples are taken from. Because of the fact that all spectra were recorded with the same setup, however, they can be compared amongst each other.

Since hyperspectral fluorescence images of minerals have not been analyzed in the English literature before, it is very interesting to take a look at the spatial differences of the emitted fluorescence spectra. As can be seen in Fig. 17.1 and Fig. 17.2, respectively, the fluorescence intensity at a considered wavelength includes very discriminative information

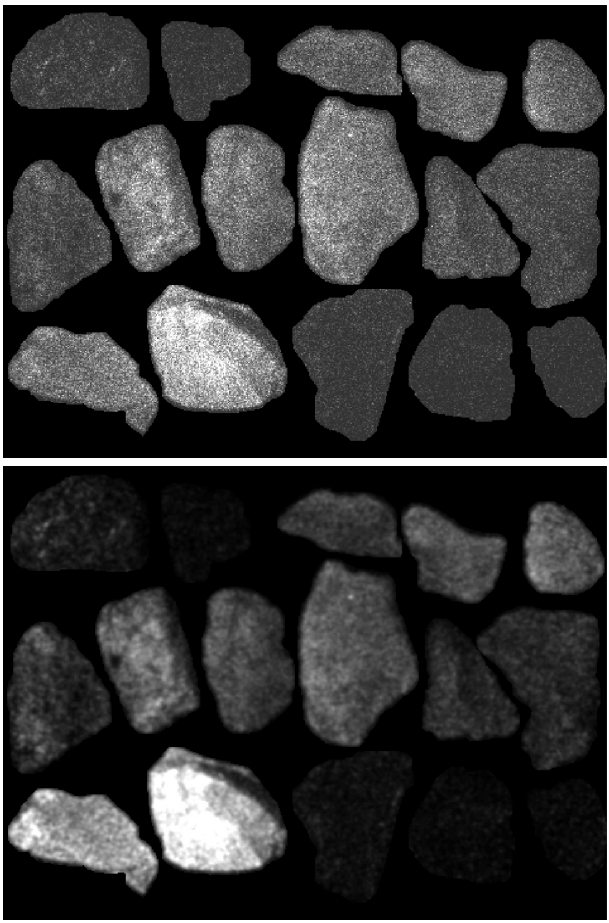

Figure 17.1: Top: Raw image of one scene at 526 nm using an excitation wavelength of 320 nm. Bottom: filtered and intensity corrected image. The background parts have been masked. Both images share the same grayscale: pixel values of 0 are shown in black, 500 in white. The samples in the top row are from left to right granite (two samples) and talc (three samples). The second row includes four samples of talc with pyrite and two yellow magnesite samples, while the last row consists of two samples of white magnesite and three chlorite samples.

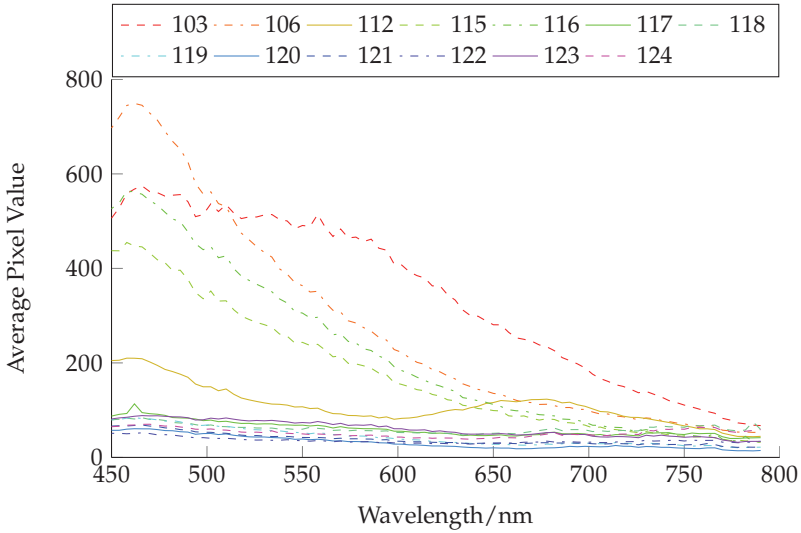

Figure 17.2: Mean spectra of the magnesite samples.

about the present minerals. Therefore, it should be investigated if the sample geometry has an impact on the measured intensity. Figure 17.3 displays two images of one magnesite. The shading used in the left image (fluorescence image at 360 nm excitation wavelength), however, is not a physical one: The color of each pixel shows the intensity of the corresponding pixel spectrum. It is interesting to note that although no change in mineral composition can be seen in the color image, there is a high illumination intensity at the breaking edge.

Figure 17.4 shows a similar picture of a dolomite sample. The green circle marks an edge with an angle of almost 90° which is relatively hard to distinguish from the adjacent surfaces, although the light comes from the viewing direction. Especially in the region highlighted in red, there is no difference between the two surfaces. The light spot on the left comes from some crust on the mineral surface which could be mortar or naturally grown. As the sample had a paper sticker attached to it, there is another white spot in the lower part of the image. From these two examples, it can be stated that the geometry can, but must not nec-

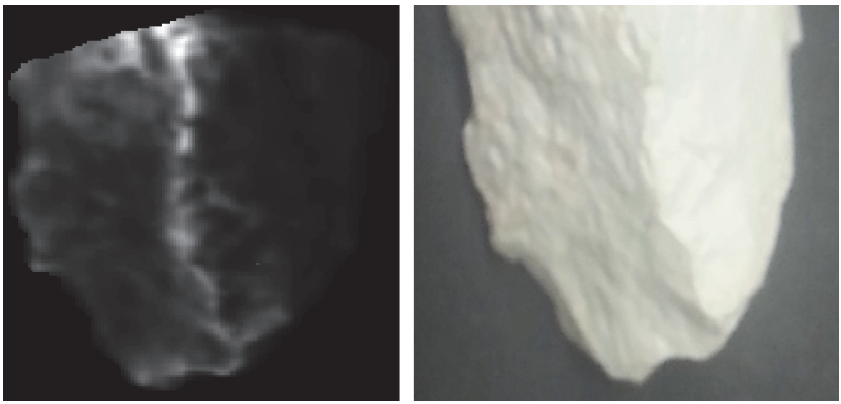

Figure 17.3: The pixel colors in the left picture show the sum of all spectral values of the considered pixels (i.e., the integral of the pixel spectrum). White indicates the highest spectral sum, while black indicates the lowest. The upper corner of the image has been cut off due to low illumination intensity. The right image is an RGB image of the same sample.

essarily have an impact on the fluorescence intensity. This fact should be considered in future sorting machines.

4 Classification and results

We already presented the classification results of a small sample [10,11], but we only used 21 wavelengths instead of 86. Due to the fact that just a small sample was considered, the classificators were trained with pixels from the same samples that were to be classified. As in the present study, hyperspectral images of more samples were acquired, we now are able to give the classification results of all minerals with at least two pieces from the same origin. Minerals of the same sort from the same origin form one class such that there are five magnesite classes and five other classes each formed by a different mineral type. We used the pixels of one mineral out of each class as training data and all other minerals from all classes as test data. This results in ten classes and one mineral of each class was selected as training sample. All other minerals from these classes were used as test data and had to be classified

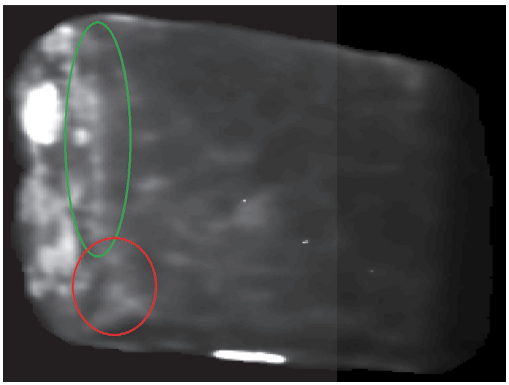

Figure 17.4: Intensity image of a dolomite sample at 360 nm excitation wavelength.

into one of the ten classes. We used three different types of classifiers: linear discriminant analysis (LDA), the k-nearest neighbors algorithm (KNN, 5 neighbors) and the spectral angle mapper (SAM) [11, 13]. The SAM classifier is invariant against illumination differences. This is due to the fact that it interprets a spectrum as a vector in the N-dimensional space with N being the number of spectral bands. It compares each pixel spectrum with one reference spectrum of each class by calculating the spectral angle between two vectors, i.e., one reference spectrum and the respective test spectrum. By the calculation of the angle, a distance measure independent of the spectrum intensity is introduced due to the fact that the spectra are divided by their norm. The reference spectra of each class are the mean spectra of the respective training samples. The training samples are not considered in the object classification rate (an object is classified as one class if most of its pixels are classified into this class). The resulting 16 minerals are classified as given in Table 17.2. All classifiers show rather low classification rates, but one should keep in mind that 10 different classes consisting of only 6 different minerals have been considered. If magnesite samples are classified incorrectly, they mostly are classified into the wrong magnesite class. This underlines that there are large spectral fluorescence differences between samples of the same type, but from different deposits. On the other hand, a

sample of a certain deposit can be more similar to another sample from a different deposit than to one sample from the same deposit. Interestingly, the SAM classifier which neglects differences in the pixel intensity does also not perform well at all illumination wavelengths.

Table 17.2: Classification results.

Excitation	LDA	KNN	SAM
260	0.56	0.75	0.63
280	0.50	0.69	0.69
300	0.38	0.50	0.75
320	0.44	0.31	0.50
340	0.44	0.31	0.25
360	0.44	0.38	0.25

5 Summary

Hyperspectral fluorescence images of 33 minerals from 6 different types have been acquired and their spectral and spatial information has been analyzed. State of the art classifiers have been applied to the pixel spectra and showed classification results that should be improved by more sophisticated classifiers. For further work improving the classification results, it would be useful to take the intensity differences due to object geometry and illumination into account. The intrinsic advantage of hyperspectral images, i.e., the knowledge of the space-dependent spectra, should also be used for improving the classification results, as texture information (see Fig. 17.1) can also be included into the classification process. Due to the high variability in the spectra from different samples, even more samples should be investigated.

References

1. H. Wotruba and H. Harbeck, "Sensor-based sorting," *Ullmann's encyclopedia of industrial chemistry*, Wiley-VCH, 2010.
2. M. Gaft, L. Nagli, Y. Groisman, and A. Barishnikov, "Industrial online raw

materials analyzer based on laser-induced breakdown spectroscopy," *Applied spectroscopy*, vol. 68, no. 9, pp. 1004–1015, 2014.

3. M. Kim, Y. Chen, P. Mehl *et al.*, "Hyperspectral reflectance and fluorescence imaging system for food quality and safety," *Transactions – American Society of Agricultural Engineers*, vol. 44, no. 3, pp. 721–730, 2001.
4. M. Gaft, R. Reisfeld, and G. Panczer, *Modern luminescence spectroscopy of minerals and materials*. Springer, 2005.
5. The fluorescent mineral society: Fluorescent minerals. [Online]. Available: http://uvminerals.org/fms/minerals
6. H. K. Noh, Y. Peng, and R. Lu, "Integration of hyperspectral reflectance and fluorescence imaging for assessing apple maturity," *Transactions of the ASABE*, vol. 50, no. 3, pp. 963–971, 2007.
7. H. Yao, Z. Hruska, R. L. Brown, and T. E. Cleveland, "Hyperspectral bright greenish-yellow fluorescence (BGYF) imaging of aflatoxin contaminated corn kernels," in *Optics East 2006*. International Society for Optics and Photonics, 2006, pp. 63 810B–63 810B.
8. M. H. Kim, T. A. Harvey, D. S. Kittle, H. Rushmeier, J. Dorsey, R. O. Prum, and D. J. Brady, "3D imaging spectroscopy for measuring hyperspectral patterns on solid objects," *ACM Transactions on Graphics (TOG)*, vol. 31, no. 4, p. 38, 2012.
9. I. Hofer, R. Huber, G. Weingrill, and K. Gatterer, "Luminescence- and reflection spectroscopy for automatic classification of various minerals," in *OCM 2013-Optical Characterization of Materials-conference proceedings*. KIT Scientific Publishing, 2013, p. 227.
10. S. Bauer and F. Puente León, "Industrielle Sortierung von Mineralen anhand von hyperspektralen Fluoreszenzaufnahmen – Potenzialbewertung," in *Forum Bildverarbeitung 2014*, F. Puente León and M. Heizmann, Eds. Karlsruhe: KIT Scientific Publishing, 2014, pp. 215–226.
11. ——, "Gewinnung und Verarbeitung hyperspektraler Fluoreszenzbilder zur optischen Mineralklassifikation," *tm - Technisches Messen*, vol. 82, no. 1, 2015.
12. S. Lefkimmiatis, A. Bourquard, and M. Unser, "Hessian-based norm regularization for image restoration with biomedical applications," *Image Processing, IEEE Transactions on*, vol. 21, no. 3, pp. 983–995, 2012.
13. F. Kruse, A. Lefkoff, J. Boardman, K. Heidebrecht, A. Shapiro, P. Barloon, and A. Goetz, "The spectral image processing system (SIPS) – interactive visualization and analysis of imaging spectrometer data," *Remote sensing of environment*, vol. 44, no. 2, pp. 145–163, 1993.